Pure Appl. Geophys. 177 (2020), 441–454

https://doi.org/10.1007/s00024-018-2077-5

Pure and Applied Geophysics

Relationship Between Seismic Electric Signals and Tectonics Derived from Dense Geoelectric Observations in Taiwan

Feng Jiang,[1] Xiaobin Chen,[1] Chien-Chih Chen,[2] and Hong-jia Chen[2]

Abstract—Some researchers have suggested that significant electromagnetic changes that can be detected prior to strong earthquakes are associated with the tectonics and subsurface structures beneath monitoring stations. Numerical simulation seems to support this phenomenon. However, to date, few field measurement data are available to address this issue. In this work, we used the shifting correlation method to analyze 2-month recordings of 20 geoelectric stations in Taiwan and found at least two stations had recorded geoelectric signals significantly correlated with known seismic events. These two stations are installed on large reverse faults, which are probably characterized by high stress concentrations before earthquakes. In addition, they share the same resistivity variation pattern, namely, a conductor layer sandwiched between two high-resistivity layers. Moreover, both stations are above the electrical resistivity boundaries, which means they have an increased probability of recording the abnormal disturbance once EM signals have been emitted from EQs. Our analysis results support the viewpoint that lateral and vertical electrical resistivity variation and conductors in the subsurface may be able to amplify seismic electric signals.

Key words: Statistical seismology, seismic electric signals, shifting correlation method, tectonics and deep structures in Taiwan.

1. Introduction

As an electromagnetic (EM) phenomenon associated with earthquakes (EQs), seismo-electromagnetic signals (SEMS) have been widely monitored and reported by authors worldwide (Han et al. 2015, 2016a, b; Okubo 2011; Saito et al. 2011, 2013; Fujinawa and Takahashi 1990; Fujinawa et al. 2011; Takahashi et al. 2005, 2007; Hattori 2004; Varotsos and Alexopoulos 1984). Although whether the SEMS can be regarded as possible EQ precusors is still under debate, a number of experiments with rock physical (Nitsan 1977; Panfilov 2014; Fujinawa and Noda 2015) and numerical simulation results (Zhang et al. 2013; Gao and Hu 2010; Gao 2013a, b; Huang 2015; Ren et al. 2012, 2014, 2016a, b; Yamazaki 2012) have shown evidence of SEMS before, during and after EQs. To explain the observed SEMS phenomena on the basis of physics, several possible mechanisms have been proposed (Johnston 1997; Park et al. 1993; Huang and Ikeya 1998). Some researchers even tried to use SEMS to predict and investigate the generation process of EQs (Contoyiannis et al. 2005; Eftaxias et al. 2010; Kalimeris 2016; Potirakis 2011; Varotsos et al. 1993).

However, it remains difficult to convince people that SEMS can be detected prior to EQs, mainly because there is no physics-based mechanism that can be used to clearly interpret all the observations. The other important reason is that we have no equipment or data processing method that can receive or identify abnormal EM changes prior to every major EQ within a reasonable time interval and distance. In some cases, we attributed these situations to the high noise level compared with the weak SEMS around the observation sites (Huang 2005) or the signal sampling frequency being inappropriate, so that EM changes could not be captured (Park 1996), while other cases may have had nothing to do with the noise level or sampling frequency. Varotsos and Lazaridou (1991) reported that one station in Greece farther from the epicenter received seismic electric signals (SES) before a moderate earthquake, but the other station

Electronic supplementary material The online version of this article (https://doi.org/10.1007/s00024-018-2077-5) contains supplementary material, which is available to authorized users.

[1] State Key Laboratory of Earthquake Dynamics, Institute of Geology, China Earthquake Administration, Beijing, China. E-mail: cxb@ies.ac.cn; cxb@pku.edu.cn

[2] Institute of Geophysics, National Central University, Jhongli, Taoyuan City, Taiwan.

closer to the epicenter did not. They called this phenomenon the selectivity of SES. Afterwards, Uyeda et al. (2000) and Orihara et al. (2012) also reported similar phenomena in that not all EQs have detectable precursory abnormal EM changes. Based on laboratory studies on different rock samples with different loading rates and compressions, Fukui et al. (2005) concluded that whether the EM radiations can be measured largely depends on both the rock type and loading condition. These reports indicate that whether SEMS can be detected or not is probably related to the location of observational stations on the earth. Stations installed in different geologic settings may result in different capacities to detect the changes in EM signals associated with EQs. Therefore, which geologic conditions of stations are most likely to allow detecting SEMS need to be studied for better monitoring and understanding of SEMS behavior. After the concept selectivity of SES was proposed and a conductive channel model was suggested to explain this phenomenon by Varotsos and Lazaridou (1991) and Varotsos et al. (1993, 1998), some numerical simulation works were done to support this notion. For example, Sarlis et al. (1999) found the electric field would be intensified within a certain region by the numerical solution of Maxwell equations on a 2D model with a reasonably conducting channel. On the basis of observations of the Izu EQ swarm, Huang and Lin (2010) extended this work to a 3D case and found that lateral electric heterogeneity with conductors in the subsurface can largely enhance the observations of the electric field from a DC dipole source at depth. So far, however, there are few works based on real measurement data to study how tectonics around stations affect the detection of SEMS.

The Taiwan island may be one of the perfect places to statistically investigate the relationship of SES receiving and tectonics with electrical resistivity structures because it has abundant EQ records, dense geoelectric observational stations and a relatively clear geologic background. A geoelectric monitoring system (GEMS), including 25 stations (Fig. 1; the details of these stations are listed in the Table in the Supplementary Material), was installed on the island in 2012 to detect and investigate the anomalous changes of the telluric current before and after EQs (Chen and Chen 2016). Benefitting from international research projects on the Taiwan arc-continent collision, such as Taiwan Integrated Geodynamics Research, a detailed database of the geology of Taiwan is available including the type of tectonics (Shyu et al. 2005a, b) and electrical resistivity structures (Bertrand et al. 2009, 2012). In this work, we attempt to determine which stations in Taiwan probably have received SEMS and then discuss what geologic features they shared. A statistical method called the shifting correlation method (SCM) (Jiang et al. 2016), proposed 2 years ago, was applied to analyze whether or not these stations had indeed received the SEMS. Then, the characteristics of the tectonics and resistivity structures around and beneath these stations in Taiwan were discussed.

2. *Tectonics Setting of Taiwan*

The Taiwan island is located at the intersection of three plates, the Eurasian plate (EP), Philippine Sea plate (PSP) and South China Sea plate. To the south, the oceanic lithosphere of the South China Sea plate subducts eastward beneath the lithosphere of the PSP at a rate of about 82 mm/year at the Manila trench (Yu et al. 1999). By contrast, to the north, the direction of subduction is the opposite at the Ryukyu subduction zone, and extension proceeds at about 30–40 mm/year in the northwest back-arc region (Shyu et al. 2005a, b). These special geodynamic conditions have made the Taiwan island one of the most tectonically active areas in the world, leading to frequent moderate and major EQs on the island (Fig. 1b). Many geologic and geophysical studies on this area have been done, and abundant information from deep to surface have been obtained in this region. Different types of active neo-tectonics have developed in the island (Fig. 1a), most of which trend NNE along the island's long axis (Shyu et al. 2005a, b). The west flank of this region hosts fold-thrust and buried faults such as the Chelungpu faults, on which the Chi-Chi EQ occurred in 1999. To the north and northeast, active normal faults are present along the periphery of the basin. The west-dipping Lishan thrust fault (LF) is an important geologic boundary in the central island. The Longitudinal Valley faults (LVF) extend along the east coast of

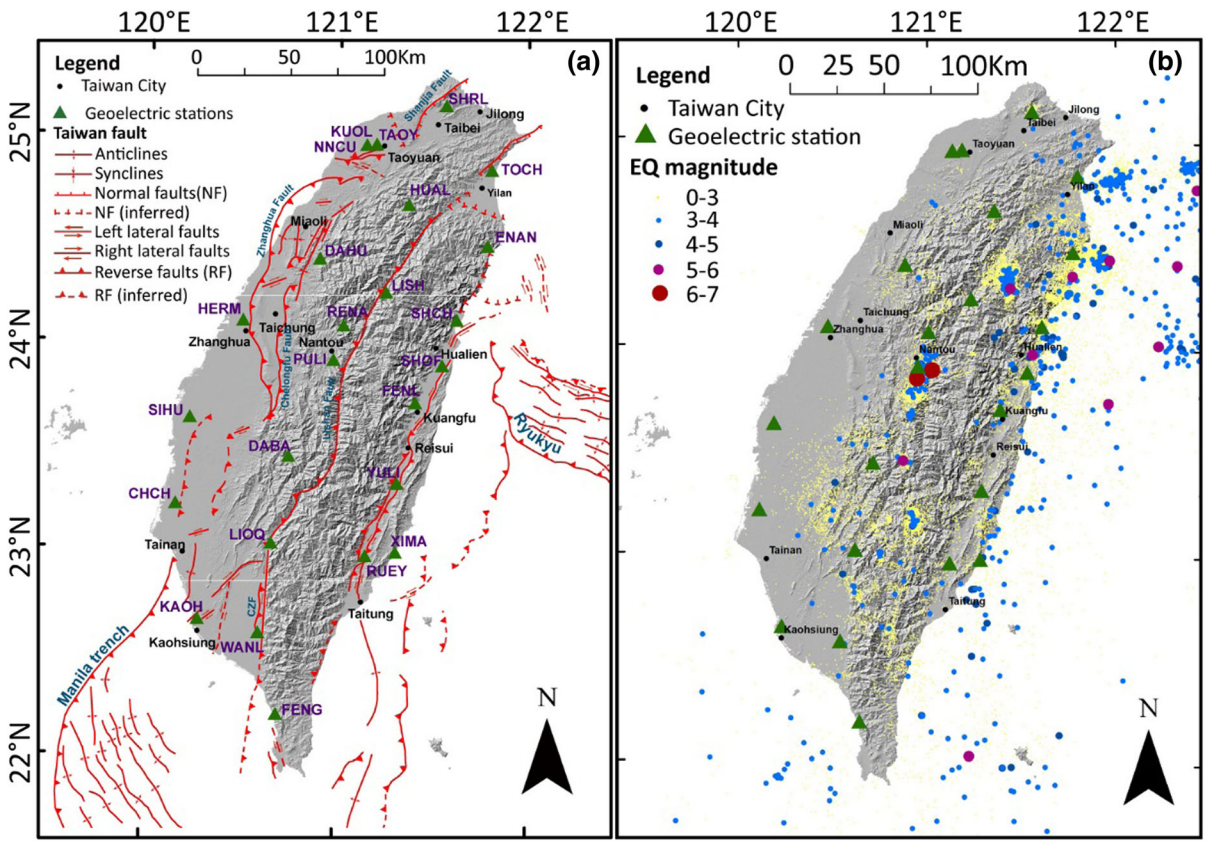

Figure 1

Topography map showing the active neo-tectonics, geoelectric monitoring system (GEMS) sites and earthquakes from 1 December 2012 to 30 June 2013 (about 6 months). **a** Neo-tectonics and GEMS sites in Taiwan and the vicinity are indicated by red lines and green triangles, respectively. Abbreviations are used for the GEMS name; more detailed information about the GEMS is provided in the Supplementary Text S1 and Table S1. **b** EQ locations represented by solid dots with different sizes and colors from the Taiwan Central Weather Bureau (http://www.cwb.gov.tw/V7e/earthquake/)

Taiwan, which is the suture belt between the EP and PSP (Yu and Kuo 2001). From south to north, its active nature changes from completely reverse in the Taidong area to dominant strike-slip in the Hualien area (Shyu et al. 2005b). Different geologic provinces are divided by these major faults and generally their ages and metamorphic grades increase to the east (Bertrand et al. 2012; Wu et al. 1997).

3. *Methods and Data*

The SCM proposed by us in 2016 (Jiang et al. 2016) is an approach to determine whether the station has received the SEMS by studying the correlation between EQs and the observed EM signals. Because it is a statistical method, two assumptions should be satisfied: (1) EQs that occurred in the same region have similar geodynamical processes and (2) the occurrence time of the SEMS relative to the EQ timing is basically similar for different EQs. The main principle of the SCM is to calculate the linear correlation of two sequences that are asynchronous changes in time. We know that pre- or post-seismic SEMS occurred before or after the timing of EQs. That is to say, EM precursors and EQs are two asynchronous sequences in time. To calculate the real pre- or post-seismic correlation between EQs and EM signals, sequences of EQs or EM signals need to be shifted with respect to each other on the time axis. Only co-seismic correlation can be

obtained without relative shifting. It is a very simple concept but permits reliably identifying the EM anomalous changes associated with EQs that are superposed in the EM time series (Jiang et al. 2016). It should be noted that the EM noises or periodic signals from space in the time series have a very low probability of having a significant correlation with EQs. This method was first applied to the aftershocks of the Minxian, China M6.5 EQ in 2013 (Jiang et al. 2016) and 1-month recordings of two MT stations close to the epicenter. Obvious time and frequency features of SEMS were obtained, which were consistent with the results from other researchers.

In this study, geoelectric recordings for 2 months from 26 February to 26 April 2013 from 20 stations in Taiwan were included. The signals recorded in this period had much lower noise and were more stable and continuous than other time period. First, sequences of correlation coefficients between EM time series and earthquakes close to the station were calculated for every station. Then, a comprehensive statistical test and analysis were carried out to determine which of the 20 stations had significant correlations indicating a large probability of recording the SES. Finally, the features of the tectonics and subsurface resistivity structures beneath those stations were discussed.

3.1. Processing of Geoelectric Field Data

The geoelectric field at every station was observed in two directions denoted by Ex and Ey in this article. They have a sampling frequency of 1 Hz. Part of the time series from the four stations is shown in Fig. 2. We found obvious periodic noise signals in the night period. Although we mentioned above that the noises and periodic signals have a low probability of having a significant correlation with EQs, artificial signals will surely make the whole correlation between EM signals and EQs lower. To obtain reliable results, it was best to delete the obvious interferences in the EM time series before applying the SCM. In this article, only recordings between 8:00 and 16:00 (local time, total of 8 h) of all 20 stations were used. The telluric current recorded during this time period had a low noise level and no obvious artificial signals.

Previous studies suggest that daily variation of EM signals can be used to study the lead time of SEMS (Han et al. 2014, 2016b; Hattori et al. 2013; Orihara et al. 2012). Following this notion, the time window of 1 day was chosen for the average geoelectric signals in this work. Consequently, 28,800 samples within 8 h per day were converted into one value, resulting in daily variation of geoelectric signals for each station. The duration of the SES was said to be at least tens of minutes or several hours (Eftaxias et al. 2001; Fujinawa and Takahashi 1990; Varotsos and Lazaridou 1991). Therefore, the processing procedures were as follows: First, we obtained a median of 60 values within every minute and then extracted the median again from 60 values within every hour. The short-time accidental noises were eliminated by doing so. Finally, we averaged the eight values within each day rather than calculating the median because we needed to keep possible SES lasting around an hour. The daily variation of 20 EM time series derived from 20 stations was prepared for the SCM in the next step. The results of data processing for FENL and HUAL stations are shown step by step in Fig. 3.

3.2. EQ Catalog Processing

The time period of EQs should be longer than the geoelectric signals to keep a stable statistical sample size when conducting the shifting correlation calculation. EQs in Taiwan Island from 1 December 2012 to 30 June 2013 were selected. For a specific station, only the EQs within 50 km of the station were used when conducting SCM because there was little chance of EM disturbance being received for the EQs far from the station (Han et al. 2014; Hattori et al. 2006). To implement the SCM, the daily variation of the EQ sequence needed to be matched with the daily variation of the geoelectric field at every station. Therefore, the target EQs needed to be converted to energy values based on their magnitudes according to the Gutenberg-Richter equation (Gutenberg and Richter 1956), and then we summed the energy of EQs on each day. Finally, the total EQ energy of each day was converted back to magnitude to generate a daily variation sequence of EQ energy around each station. This EQ sequence is called the

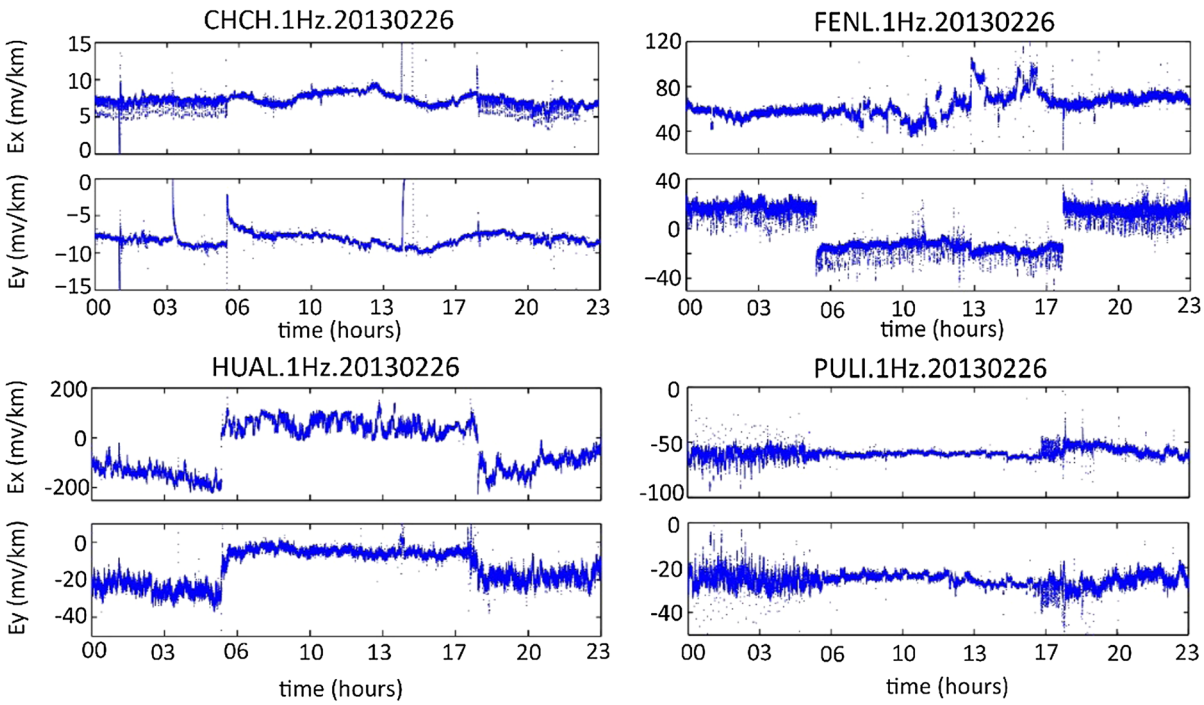

Figure 2
Time series (TS) sampled at 1 Hz on 26 February 2013 from four stations (CHCH, PULI, HUAL, FENL). Names, samplings and dates of these TS are shown in the titles. Each station includes variations of the two Ex (upper) and Ey (below) components. Only recordings between 8:00 and 16:00 (local time) of all 20 stations were used in the research

"equivalent EQ" sequence and denoted as Meq. More details about this can be found in Jiang et al. (2016). The example of the Meq variation for the HUAL station is presented in the Fig. 4, which clearly shows that the Meq sequence can represent the real variation of the EQ energy around a station.

3.3. *Shifting Correlation Calculation*

For every station, the Meq sequence was fixed in time. The synchronous time of two sequences was the shifting start point. The geoelectric sequence was shifted to the right or left continuously day by day with respect to the fixed Meq sequence. Meanwhile, the linear correlation coefficients between Meq and EM sequences were calculated at different shifts, termed the shifting correlation coefficients (SCCs) of each station. Considering this would compare the values of SCCs derived from different stations, the daily variation of geoelectric signals from each station was normalized by its own mean and variance before implementing SCM. Obviously, the co-seismic correlation coefficient of two sequences can be calculated without any shifting; thus, "0" was marked on the shifting time axis. The values calculated from left-/rightward shifting with respect to Meq were marked by positive/negative values written on the right/left side of the shifting time axis as post-/pre-seismic correlation coefficients. Therefore, the degree of correlation between EQ energy and geoelectric signals in three seismic stages could be reflected by the SCCs simultaneously, i.e., before, during and after EQs. The values of SCCs at each station also indicated the probability of the existence of the SES. That means a larger value indicated a higher likelihood of the existence of the SES within the monitoring EM signals, and the corresponding shifting time indicated the statistical occurrence time of the SES. According to previous works, the pre-seismic ULF SES more likely occurred several days or several weeks before EQs (Han et al. 2014; Hattori et al. 2013; Jiang et al. 2016; Xu et al. 2013).

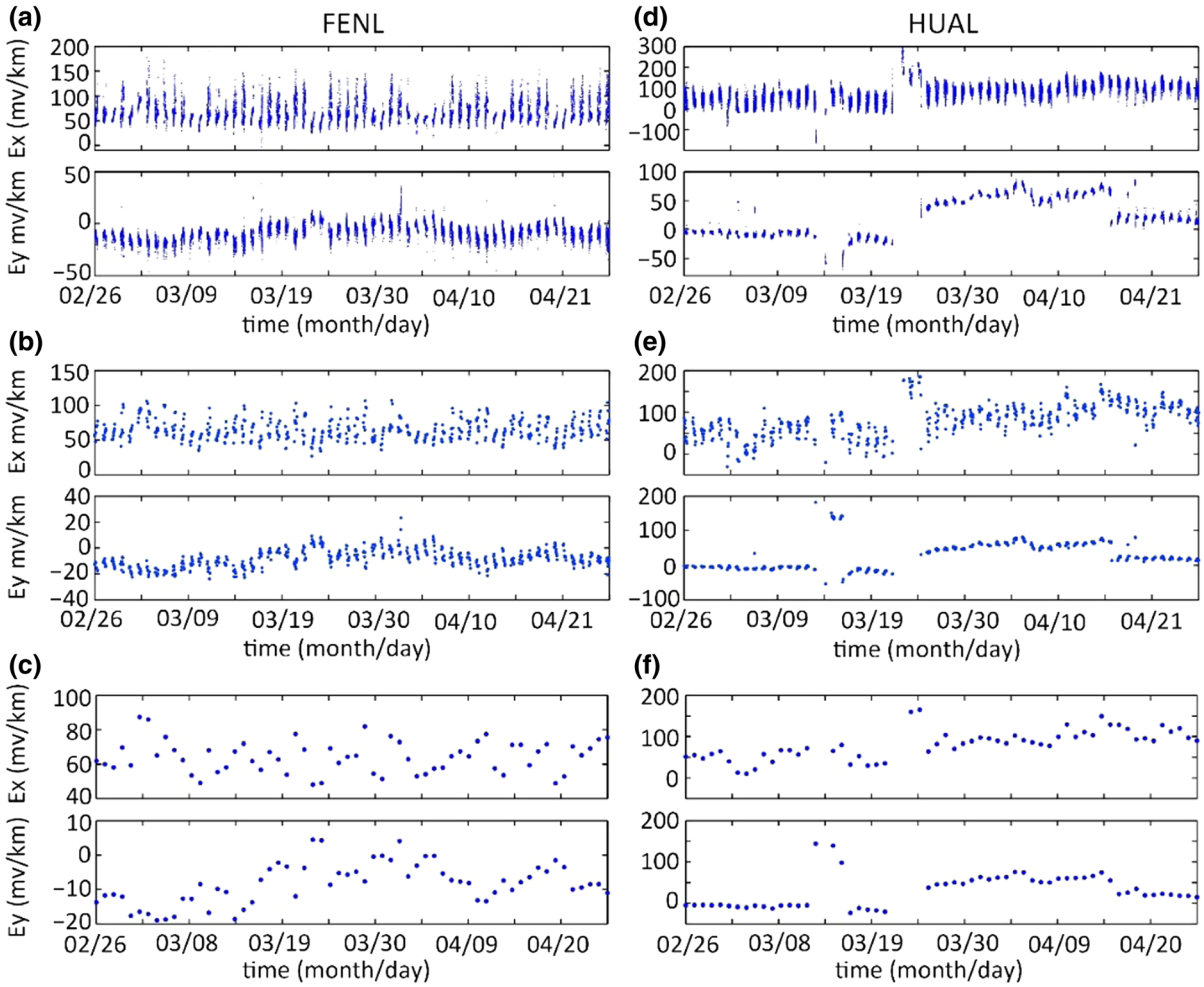

Figure 3
Data processing results of each step. **a–c** Variations of a value per minute, hour and day, respectively, in FENL. **d–f** Same variations as for FENL but for HUAL station

Therefore, right- and leftward shifting 60 days from the co-seismic time was used for every station to investigate the correlation between EQs and geoelectric signals. As examples, Fig. 5 shows the SCCs calculated at FENL and HUAL stations. The variations of SCCs in Ex and Ey polarization are shown at each station. We found that the variation of SCCs was quite different between Ex and Ey at FENL station, but more consistent at HUAL station where we can see high values in two sections located around 24 days before (− 24) and 16 days after (16). There are low co-seismic timing values at the two stations. The SCC results for the rest of the 18 stations are shown in Figure S1 in the Supplementary Materials.

Because high correlation coefficients in SCCs were used to determine whether the station had recorded the SES, two significant test methods were carried out to ensure that the high correlation values in the SCCs of each station were statistically significant. The first was to implement the SCM on two random sequences that have the same number of samples as the real Meq sequence and daily variation of geoelectric signals, respectively. One hundred twenty-one correlation values were obtained for every random sequence pair. We obtained the

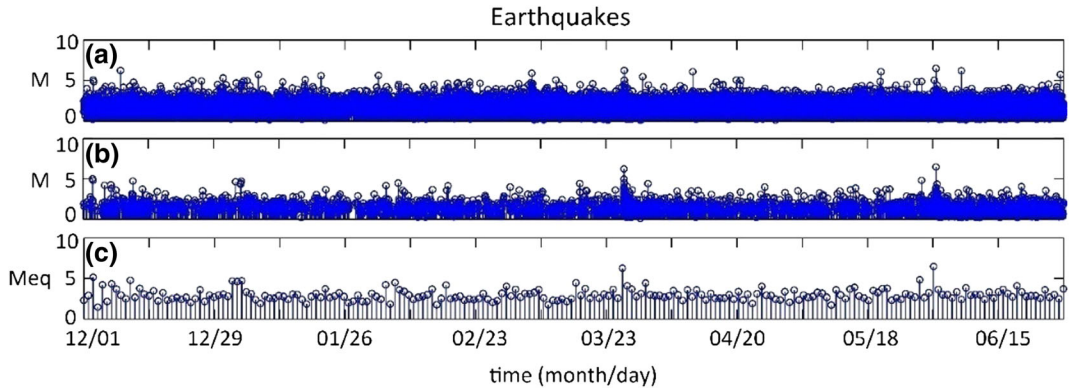

Figure 4
Equivalent EQ (Meq) sequence of HUAL station. **a** Entire EQ catalog of Taiwan Island from 1 December 2012 to 30 June 2013. **b** EQs within 50 km of HUAL station. **c** Equivalent EQs converted from **b**

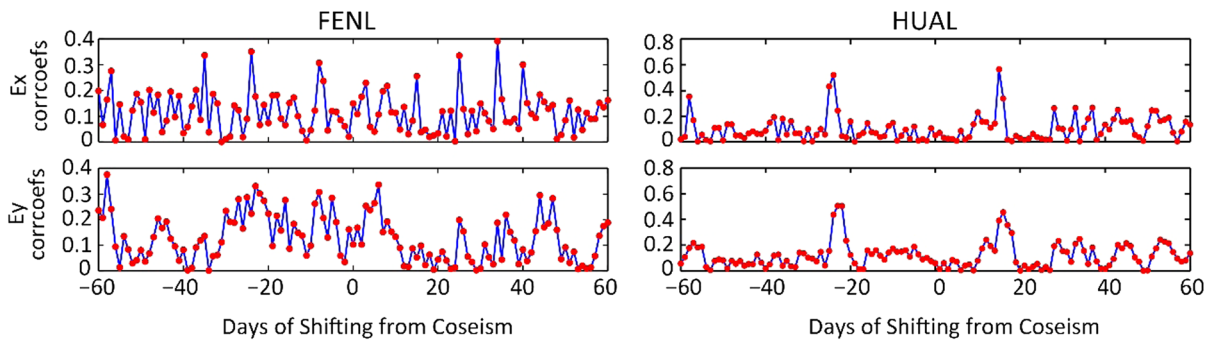

Figure 5
Variations of shifting correlation coefficients (SCCs) for FENL and HUAL stations. Horizontal axis indicates the days of shifting of geoelectric signals from the coseismic with respect to the Meq sequence. Positive values denote the days of right shifting; negative values denote the days of left shifting. '0' means coseismic having no shifting. Vertical axis corresponds to the values of SCCs marked by 'corrcoefs' in the label. The title on the top of each figure is name of the station

absolute values of these 121 correlation coefficients and then picked out their maximum. This test procedure was repeated 100,000 times, and the distribution of the maximum correlation coefficients in each test is plotted in Fig. 6a. The second test was to avoid the high SCCs in a certain shifting day caused by the special daily variation of the geoelectric sequence. Therefore, on the basis of the original catalog, a random EQ catalog was needed to carry out this test. We let the locations of the EQs have uniform random distribution within the space constrained by the original EQ catalog, but kept their original magnitudes. For the timings, we replaced the hours, minutes and seconds of the EQs by random values, but kept their years, months and days. Thus, a new EQ catalog with the same size as the original one was constructed, called the 'random EQ catalog' in this article. Then, we calculated SCCs for each station using the random EQ catalog and real observed geoelectric signals. This test was repeated 100 times for each station. Thus, 100 values were obtained for every single shifting day in the SCC sequence. Taking HUAL station as an example, the second test results are plotted in Fig. 6b. To ensure 100 random computations were enough for the second test, 1000 repeats were done in the Ex component of FENL and HUAL stations. The results are shown in Figure S2 in the Supplementary Material. Comparing the two results (100 and 1000 test times), they had almost the same variation trend

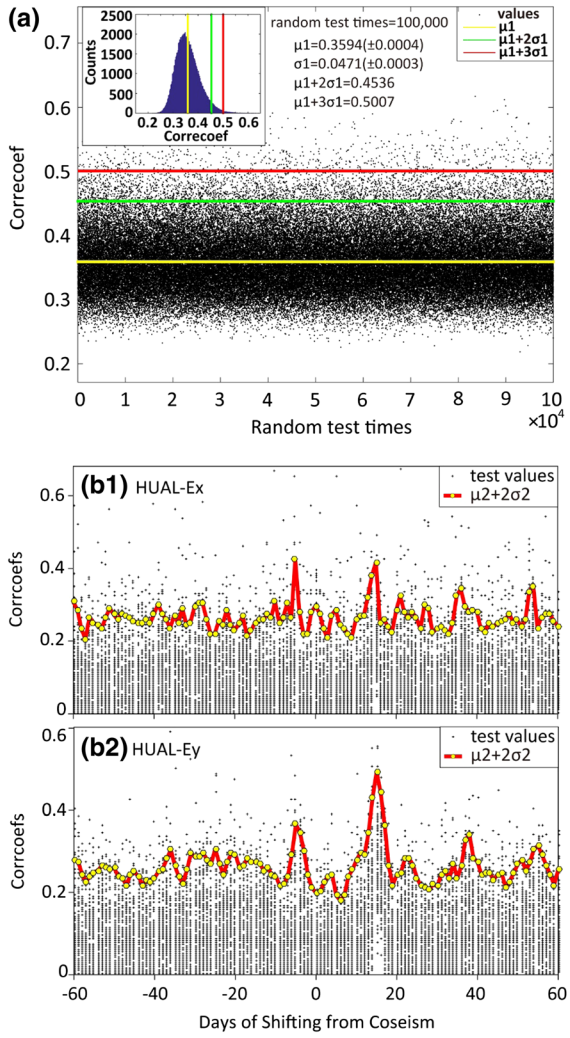

Figure 6
Results of two statistically significant tests. **a** Distribution of maximum correlation coefficients among 121 values for 100,100 random tests. The frequency distribution diagram is plotted in the left upper corner. Yellow horizontal lines are median value (μ_1); green and red lines are the mean value (μ_1) plus two and three times the standard deviation (σ_1), respectively. The numbers in parentheses are their uncertainties. **b** Significant tests for every single shifting correlation coefficient in the SCC sequence of each station. Ex and Ey of HUAL station as an example are shown in **b1** and **b2**. There were 100 values in every single shifting day, indicated by black crosses; their mean value (μ_2) plus two times the standard deviation (σ_2) is represented by yellow solid dots with red strings

for the mean values and standard deviation curves, except the curves from 1000 times were flatter when there was no abnormal change. Hence, the 100 computations were enough to make the second test valid. Actually, we just randomly changed the locations of the original EQs in the second test. Therefore, it should be emphasized that the second test was applied to see if the single high SCC in an SCC sequence was probably caused by the special daily variation of geoelectric signals, whereas the first test was carried out to evaluate the statistical significance of the high values. As shown in Fig. 2b, the variation of two times the standard deviation (SD) threshold had peaks on certain shifting days from coseismic. This probably meant these days could inherently have high SCCs. We should be careful when high values occur in these shifting days in the real results, such as around 5 days before and 15 days after at HUAL station (Figs. 5, 6).

4. Results and Discussion

After the SCCs for every station had been obtained, two random tests were applied to select the stations with significant correlations, indicating the EM signals associated with EQs had been received. Mean value (μ_1) plus three times the standard (σ_1) deviation and mean value (μ_2) plus two times the standard (σ_2) deviation were chosen as the references for the first and second random tests, respectively. Both are plotted together with the real SCCs of each station. The results are shown in Figure S3 in the Supplementary Material. Significant correlations were found at least in the two stations shown in Fig. 3. HUAL and RUEY stations revealed considerable correlations between EQs and EM signals around 23 days and 37 days before EQs where values not only exceeded $\mu_1 + 3\sigma_1$ but also had no inherently high correlation around these times. Although there was high correlation around 15 days afterward at HUAL station, the results of the second random test also showed relatively high values around the same time. Therefore, we think the two preseismic significant correlations were reliable and indicate that these two stations had detected the preseismic EM signals related to the EQs. The occurrence times of these preseismic signals were consistent with our previous result of 23 days before EQs, which used the same method on Minxian-Zhangxian M6.5 EQ (Jiang et al. 2016), and in agreement with studies of other researchers using different methods on different

single EQs in different countries. For instance, Varotsos and Lazaridou (1991) and Varotsos et al. (Varotsos et al. 1993) got preseismic EM signals 3 weeks before the EQs in Greece; Orihara et al. (2012) suggested that SES are more likely to be detected within 30 days before EQs. Hattori et al. (2013) presented the anomalies associated with EQs that occurred 3–4 weeks before events. Hayakawa et al. (2015) reported ULF geomagnetic disturbances 2–4 weeks before the M7.9 Wenchuan, China, EQ in 2008. Previous studies on the occurrence time of SEMS convinced us further that these two stations in Taiwan recorded the preseismic geoelectric signals related to EQs. We also recognize that the co-seismic correlation (indicated by '0' on the horizontal axis) at all the stations were low and had no significance. The reason is probably the short duration of co-seismic SES (< 1 h), which results in weak coseismic signals during time series processing when converting raw data to diurnal variation. Besides, it is not impossible that all stations indeed did not record any co-seismic SES. The absence of co-seismic SES for some considerable EQs in long-term observations is an important reason why the existence of SEMS is questioned (Geller 1997; Uyeda et al. 2009). Many authors reported co-seismic SEMS, but most arrived at the station along with seismic waves not produced directly from the focus (Tang et al. 2010; Ujihara et al. 2004) (Fig. 7).

In this scenario, it is believable that at least 2 out of 20 stations in Taiwan identified credible statistically significant correlations before EQs. The rest of the stations may just detect weak signals before EQs compared with the background EM signals from space, which could not be identified by our method in this article. However, we were able to investigate what geologic features of these two stations are favorable to receiving significant geoelectric signals related to EQs. First, the results in Fig. 8a show that both are installed on the large reverse faults, which are the Lishan and Longitudinal Valley suture zones, respectively (Shyu et al. 2005a, b). These not only have high stress concentrations, but also are located above geologic tectonic boundaries. The rocks on either side were built by different tectonic activities in different ages. Second, the 2D and 3D magnetotelluric (MT) inversion results (Bertrand et al. 2009, 2012) (Figures S4–6) were used here for discussion. As shown in Fig. 8a, HUAL station is exactly on the north MT profile; RUEY station is close to the south profile with a distance of about 10 km. This means the MT data can constrain the electrical resistivity beneath these two stations well. The 2D resistivity models of the north and south profiles (Fig. 8b revealed that a big conductor is right beneath the HUAL station. For RUEY station, we could not see any obvious abnormal resistivity structures (Fig. 8b2). To get more detailed electric information on these two stations, the resistivity changing curves right beneath the two stations were extracted from 3D MT models (Fig. 8c). Both showed rich changes in resistivity with depth. It is notable that they share the same resistivity pattern. The changes were high-low-high-low-high resistivity from the surface to deep subsurface. This pattern reveals multiple electrical interfaces under the

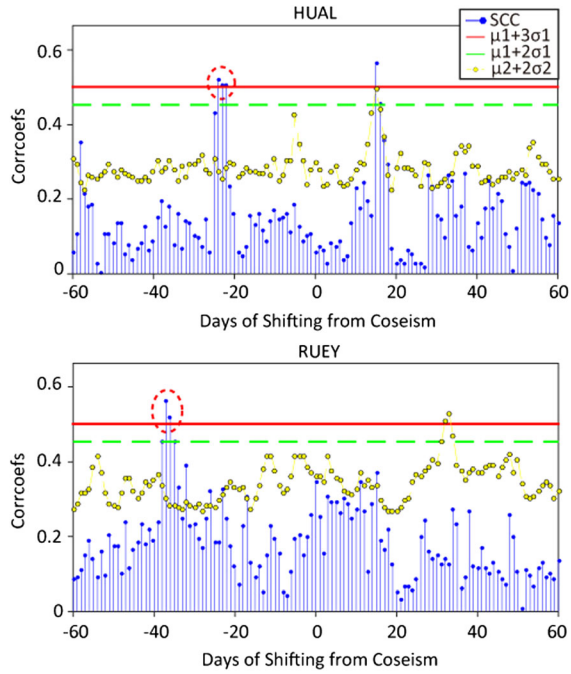

Figure 7
Two stations had significant correlations between EQs and geoelectric signals. The shifting correlation coefficients in each station were plotted by blue bars; red and light green lines are mean value plus three and two times the standard deviation of the first random test. Variation of the mean value plus two times the standard deviation of the second random test was represented by yellow dots. The dashed ellipses highlight the significant correlations in two stations

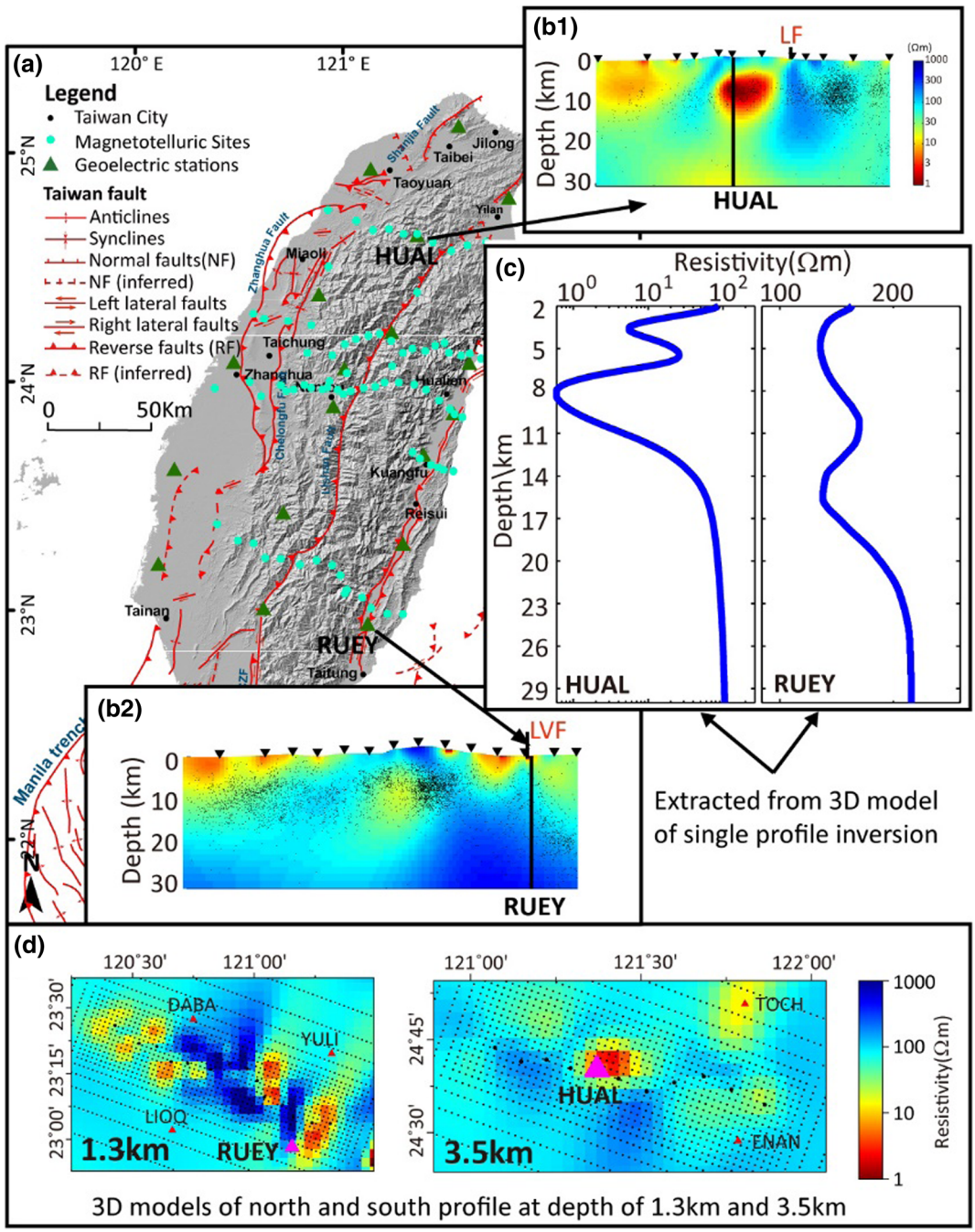

Figure 8

Tectonics and magnetotelluric models in Taiwan Island. **a** Distributions of tectonics and locations of geoelectric monitoring stations involved in this article are indicated by green triangles, and magnetotelluric sites are denoted by light green solid dots distributed in northern, central and southern Taiwan, respectively. **b1**, **2** The 2D electrical resistivity model with a black vertical line denotes the location of HUAL and RUEY stations. EQs from 30 October 2012 to 31 October 2013 within 20 km of the profiles were projected onto the models, which were denoted by small black dots. LF represents the Lishan Thrust faults. LVF is the location of the Longitudinal Valley faults. **c** Electrical resistivity variation beneath two stations extracted from 3D models of single profile inversion. **d** Horizontal slices at 1.3 km and 3.5 km depth from the 3D models of the northern and southern MT profiles

stations, especially HUAL station. In the horizontal map (Fig. 8d), we can see HUAL and RUEY stations are located around the electrical boundary in the shallow portion at 1.3 km and 3.5 km depth, respectively. Besides, the 3D P-wave seismic tomography results (Hsu 2001; Sibuet and Hsu 2004) indicated that HUAL station is right above the position where abrupt velocity changes occur at 15 km depth.

For the other stations located relatively close to the MT profiles, we also obtained the electrical resistivity changing curves beneath them (Figure S7), all of which were picked out from the center of Taiwan where more MT data were available to constrain the deep electrical structure well. Even though most of them are installed above the reverse faults too, they did not show obvious shallow conductors, such as HUAL and RUEY stations, or significant electrical interfaces at depth. HERM is located above the western basin characterized by a thick conductive layer (Bertrand et al. 2012) at the top surface, which is a disadvantage for receiving signals from hypocenters. We found that PULI station does have a relative conductor at about 9.5 km depth, but has a low chance of receiving the SEMS according to our previous statistical analysis. The conductor beneath PULI station is much deeper than that at HUAL station, which is the most obvious difference between the two. Is this telling us the shallower conductor and more electrical interfaces beneath the observational stations play an important role in receiving the SEMS? Further work needs to be done on PULI station, e.g., on more detailed 3D electrical resistivity beneath it, which will help interpret this phenomenon.

To sum up, this study suggests that the HUAL and RUEY stations in Taiwan, which have recorded preseismic EQ-related geoelectric signals, are on large reverse faults where a high stress concentration probably exists during the EQ preparation stage. In addition, all the features of deep structures revealed that both stations are located above geologic and electrical resistivity boundaries. These conditions are favorable for acquiring high signal and noise data. Because the intensity of the electrical field will be enhanced around the electrical boundary because of charge effects, at these places stations can record the high and stable background electric field. Once extra EM signals have been emitted from EQs and superposed on the recordings, these abnormal disturbances will be easy to identify. To some extent, these conditions are also supported by the modeling studies of Huang and Lin (2010), who reported that surface inhomogeneity and conductors beneath the resistivity surface are two important factors to enhance the intensity of the electric field from a DC electric dipole.

It is a good start to investigate the relationship between the SEMS and geologic conditions on the basis of real measurements. Although the stations under analysis have not found significant geoelectric signals related to EQs, we cannot say that they received no SES. This may just be because the SES at these stations are weak and could not be detected by our method. In future work, different methods of identifying seismic signals and observation data for much longer times should be used to further address this issue. In addition, the characteristics of EQs, such as the locations and rupture process, will be taken into consideration. Finally, we think the regions where detailed information about the subsurface structure is available should be helpful to better understand the behavior of SEMS in practice.

5. *Conclusions*

We propose that comprehensively analyzing the geologic characteristics around observational stations is important if we want to determine the reason that not every moderate EQ's preseismic EM signals can be captured. Because Taiwan Island has relatively simple tectonics, many EQs and detailed geologic knowledge data available, it is a perfect place for studying this topic with a statistics-based approach. We calculated shifting correlation coefficients (SCCs) between EQs and geoelectric signals from 20 stations in Taiwan. Finally, confined by two kinds of statistically significant random tests, two stations were found to have recorded geoelectric signals significantly related to EQs. Their occurrence time was around 23 days before EQs at HUAL station and 37 days before at RUEY station, respectively, in perfect agreement with our previous results and those

of other authors' studies in different areas using different approaches. Both stations are located on large reverse faults presumably characterized by high stress concentrations during the EQ preparation stage. More attention should be paid to the fact that they not only share the same resistivity changing pattern with depth, but also both are installed above geologic and electrical resistivity boundaries where recording higher signal-to-noise data is more likely if EM signals are emitted from EQs.

Acknowledgements

We would like to express sincere appreciation to the anonymous reviewers whose comments are important to improving our manuscript. This research was supported by the Natural Science Foundation of China (no. 41574066) as well as grants from the State Key Laboratory of Earthquake Dynamics of China. The first author, Feng Jiang, did all the specific data processing and analysis, figure making, paper writing and editing. The main idea described in this article was proposed by the corresponding author, Xiaobin Chen, and he is also advisor to the first author. The third and fourth authors provided all the original data and made some comments. We thank PhD student Benjamin Lee of the University of Alberta for his time spent correcting the language mistakes in the original paper and making some comments to improve this paper. We appreciate Prof. Martyn Unsworth and his former student Ted Bertrand of the University of Alberta who provided all the 2D and 3D MT inversion models for this article. We thank Prof. Xianglin Gao for reading and polishing the language. All the data used are listed in the references, tables and supplements. Some other detailed information about the data is provided in the supporting information.

References

Bertrand, E., Unsworth, M., Chiang, C. W., Chen, C. S., Chen, C. C., Wu, F., et al. (2009). Magnetotelluric evidence for thick-skinned tectonics in central Taiwan. *Geology, 37*(8), 711–714. https://doi.org/10.1130/g25755a.1.

Bertrand, E. A., Unsworth, M. J., Chiang, C.-W., Chen, C.-S., Chen, C.-C., Wu, F. T., et al. (2012). Magnetotelluric imaging beneath the Taiwan orogen: An arc-continent collision. *Journal of Geophysical Research*, *117*, B01402. https://doi.org/10.1029/2011JB008688

Chen, H.-J., & Chen, C.-C. (2016). Testing the correlations between anomalies of statistical indexes of the geoelectric system and earthquakes. *Natural Hazards, 84*(2), 877–895.

Contoyiannis, Y., Kapiris, P., & Eftaxias, K. (2005). Monitoring of a preseismic phase from its electromagnetic precursors. *Physical Review E, 71*(6), 066123.

Eftaxias, K., Balasis, G., Contoyiannis, Y., Papadimitriou, C., Kalimeri, M., Athanasopoulou, L., et al. (2010). Unfolding the procedure of characterizing recorded ultra low frequency, kHz and MHz electromagnetic anomalies prior to the L'Aquila earthquake as pre-seismic ones-Part 2. *Natural Hazards and Earth System Science, 10*(2), 275–294.

Eftaxias, K., Kapiris, P., Polygiannakis, J., Bogris, N., Kopanas, J., Antonopoulos, G., et al. (2001). Signature of pending earthquake from electromagnetic anomalies. *Geophysical Research Letters, 28*(17), 3321–3324.

Fujinawa, Y., & Noda, Y. (2015). Characteristics of seismoelectric wave fields associated with natural microcracks. *Pure and Applied Geophysics, 173*(1), 255–268. https://doi.org/10.1007/s00024-015-1043-8.

Fujinawa, Y., & Takahashi, K. (1990). Emission of electromagnetic radiation preceding the Ito seismic swarm of 1989. *Nature, 347*(6291), 376–378.

Fujinawa, Y., Takahashi, K., Noda, Y., Iitaka, H., & Yazaki, S. (2011). Remote detection of the electric field change induced at the seismic wave front from the start of fault rupturing. *International Journal of Geophysics*. https://doi.org/10.1155/2011/752193.

Fukui, K., Okubo, S., & Terashima, T. (2005). Electromagnetic radiation from rock during uniaxial compression testing: the effects of rock characteristics and test conditions. *Rock Mechanics and Rock Engineering, 38*(5), 411–423.

Gao, Y., Chen, X., Hu, H., & Zhang, J. (2013a). Early electromagnetic waves from earthquake rupturing. I. Theoretical formulations. *Geophysical Journal International, 192*(3), 1288–1307.

Gao, Y., Chen, X., Hu, H., & Zhang, J. (2013b). Early electromagnetic waves from earthquake rupturing. II. Validation and numerical experiments. *Geophysical Journal International, 192*(3), 1308–1323.

Gao, Y., & Hu, H. (2010). Seismoelectromagnetic waves radiated by a double-couple source in a saturated porous medium. *Geophysical Journal International, 181*(2), 873–896.

Geller, R. J. (1997). Earthquake prediction: a critical review. *Geophysical Journal International, 131*(3), 425–450. https://doi.org/10.1111/j.1365-246X.1997.tb06588.x.

Gutenberg, B., & Richter, C. F. (1956). Magnitude and energy of earthquakes. *Annals of Geophysics., 9,* 1–15.

Han, P., Hattori, K., Hirokawa, M., Zhuang, J., Chen, C. H., Febriani, F., et al. (2014). Statistical analysis of ULF seismomagnetic phenomena at Kakioka, Japan, during 2001–2010. *Journal of Geophysical Research: Space Physics, 119*(6), 4998–5011.

Han, P., Hattori, K., Huang, Q., Hirooka, S., & Yoshino, C. (2016a). Spatiotemporal characteristics of the geomagnetic diurnal variation anomalies prior to the 2011 Tohoku earthquake (Mw 9.0) and the possible coupling of multiple pre-earthquake phenomena. *Journal of Asian Earth Sciences, 129,* 13–21.

Han, P., Hattori, K., Xu, G., Ashida, R., Chen, C.-H., Febriani, F., et al. (2015). Further investigations of geomagnetic diurnal variations associated with 2011 off the Pacific coast of Tohoku earthquake (Mw 9.0). *Journal of Asian Earth Sciences, 114,* 321–326.

Han, P., Hattori, K., Zhuang, J., Chen, C.-H., Liu, J.-Y., & Yoshida, S. (2016b). Evaluation of ULF seismo-magnetic phenomena in Kakioka, Japan by using Molchan's error diagram. *Geophysical Journal International*, *208*, 482–490.

Hattori, K. (2004). ULF geomagnetic changes associated with large earthquakes. *Terrestrial, Atmospheric and Oceanic Sciences, 15,* 329–360.

Hattori, K., Han, P., Yoshino, C., Febriani, F., Yamaguchi, H., & Chen, C.-H. (2013). Investigation of ULF seismo-magnetic phenomena in Kanto, Japan during 2000–2010: case studies and statistical studies. *Surveys in Geophysics, 34*(3), 293–316.

Hattori, K., Serita, A., Yoshino, C., Hayakawa, M., & Isezaki, N. (2006). Singular spectral analysis and principal component analysis for signal discrimination of ULF geomagnetic data associated with 2000 Izu Island Earthquake Swarm. *Physics and Chemistry of the Earth, Parts A/B/C, 31*(4), 281–291.

Hayakawa, M., Schekotov, A., Potirakis, S. M., Eftaxias, K., Li, Q., & Asano, T. (2015). An integrated study of ULF magnetic field variations in association with the 2008 Sichuan Earthquake, on the basis of statistical and critical analyses. *Open Journal of Earthquake Research, 4*(03), 85.

Hsu, S.-K. (2001). Subduction/collision complexities in the Taiwan-Ryukyu junction area: Tectonics of the northwestern corner of the Philippine Sea plate. *Terrestrial, Atmospheric and Oceanic Sciences, 2,* 209–230.

Huang, Q. (2005). The state-of-the-art in seismic electromagnetic observation. *Recent Development in Word Seismology,* 11(Serial No. 323). (**in Chinese**)

Huang, Q., & Ikeya, M. (1998). Seismic electromagnetic signals (SEMS) explained by a simulation experiment using electromagnetic waves. *Physics of the Earth and Planetary Interiors, 109*(3), 107–114.

Huang, Q., & Lin, Y. F. (2010). Numerical simulation of selectivity of seismic electric signal and its possible influences. *Chinese Journal of Geophysics-Chinese Edition, 53*(3), 535–543.

Huang, Q., Ren, H. X., Dan, Z., & John, C. Y. (2015). Medium effect on the characteristics of the coupled seismic and electromagnetic signals. *Proceedings of the Japan Academy. Series B, Physical and Biological Sciences, 91*(1), 17.

Jiang, F., Chen, X., Zhan, Y., Zhao, G., Yang, H., Zhao, L., et al. (2016). Shifting correlation between earthquakes and electromagnetic signals: a case study of the 2013 Minxian-Zhangxian M L 6.5 (M W 6.1) earthquake in Gansu. *Pure and Applied Geophysics, 173*(1), 269–284.

Johnston, M. (1997). Review of electric and magnetic fields accompanying seismic and volcanic activity. *Surveys In Geophysics, 18*(5), 441–476.

Kalimeris, A., Potirakis, S. M., Eftaxias, K., Antonopoulos, G., Kopanas, J., & Nomikos, C. (2016). Multi-spectral detection of statistically significant components in pre-seismic electromagnetic emissions related with Athens 1999, M = 5.9 earthquake. *Journal of Applied Geophysics, 128,* 41–57.

Nitsan, U. (1977). Electromagnetic emission accompanying fracture of quartz-bearing rocks. *Geophysical Research Letters, 4*(8), 333–336.

Okubo, K., Takeuchi, N., Utsugi, M., Yumoto, K., & Sasai, Y. (2011). Direct magnetic signals from earthquake rupturing: Iwate-Miyagi earthquake of M 7.2. *Japan. Earth and Planetary Science Letters, 305*(1–2), 65–72.

Orihara, Y., Kamogawa, M., Nagao, T., & Uyeda, S. (2012). Preseismic anomalous telluric current signals observed in Kozushima Island, Japan. *Proceedings of the National Academy of Sciences, 109*(47), 19125–19128.

Panfilov, A. A. (2014). The results of experimental studies of VLF-ULF electromagnetic emission by rock samples due to mechanical action. *Natural Hazards and Earth System Sciences, 14*(6), 1383–1389. https://doi.org/10.5194/nhess-14-1383-2014.

Park, S. K. (1996). Precursors to earthquakes: Seismoelectromagnetic signals. *Surveys in Geophysics, 17*(4), 493–516.

Park, S. K., Johnston, M. J., Madden, T. R., Morgan, F. D., & Morrison, H. F. (1993). Electromagnetic precursors to earthquakes in the ULF band: A review of observations and mechanisms. *Reviews of Geophysics, 31*(2), 117–132.

Potirakis, S., Minadakis, G., & Eftaxias, K. (2011). Relation between seismicity and pre-earthquake electromagnetic emissions in terms of energy, information and entropy content, arXiv preprint arXiv:1112.5742.

Ren, H., Chen, X., & Huang, Q. (2012). Numerical simulation of coseismic electromagnetic fields associated with seismic waves due to finite faulting in porous media. *Geophysical Journal International, 188*(3), 925–944.

Ren, H., Huang, Q., & Chen, X. (2016a). Existence of evanescent electromagnetic waves resulting from seismoelectric conversion at a solid-porous interface. *Geophysical Journal International, 204*(1), 147–166. https://doi.org/10.1093/gji/ggv400.

Ren, H., Huang, Q., & Chen, X. (2016b). Numerical simulation of seismo-electromagnetic fields associated with a fault in a porous medium. *Geophysical Journal International, 206*(1), 205–220.

Ren, H., Wen, J., Huang, Q., & Chen, X. (2014). Electrokinetic effect combined with surface-charge assumption: a possible generation mechanism of coseismic EM signals. *Geophysical Journal International, 200*(2), 837–850.

Saito, S., Hattori, K., Kaida, D., Yoshino, C., Han, P., & Febriani, F. (2013). Detection and reduction of precipitation effects in geoelectrical potential difference data. *Electrical Engineering in Japan (English translation of Denki Gakkai Ronbunshi), 182,* 1–8.

Saito, S., Kaida, D., Hattori, K., Febriani, F., & Yoshino, C. (2011). Signal discrimination of ULF electromagnetic data with using singular spectrum analysis—an attempt to detect train noise. *Natural Hazard and Earth System Sciences, 11,* 1863–1874. https://doi.org/10.5194/nhess-11-1863-2011.

Sarlis, N., Lazaridou, M., Kapiris, P., & Varotsos, P. (1999). Numerical model of the selectivity effect and the V/L criterion. *Geophysical Research Letters, 26*(21), 3245–3248.

Shyu, J. B. H., Sieh, K., & Chen, Y.-G. (2005a). Tandem suturing and disarticulation of the Taiwan orogen revealed by its neotectonic elements. *Earth and Planetary Science Letters, 233*(1), 167–177.

Shyu, J. B. H., Sieh, K., Chen, Y. G., & Liu, C. S. (2005b). Neotectonic architecture of Taiwan and its implications for future large earthquakes. *Journal of Geophysical Research: Solid Earth*, *110*, B08402. https://doi.org/10.1029/2004JB003251.

Sibuet, J.-C., & Hsu, S.-K. (2004). How was Taiwan created? *Tectonophysics, 379*(1–4), 159–181.

Takahashi, I., Hattori, K., Harada, M., Isezaki, N., & Nagao, T. (2005). ULF electromagnetic environment at Southern Boso Peninsula: Signal discrimination of the geoelectromagnetic data. *IEEJ Transactions on Fundamentals and Materials, 125*(7), 583–590.

Takahashi, I., Hattori, K., Harada, M., Yoshino, C., & Isezaki, N. (2007). Anormalous geoelectrical signals observed at Southern Boso Peninsula, Japan. *Annals Geophysics, 50,* 123–135.

Tang, J., Zhan, Y., Wang, L.-F., Dong, Z.-Y., Zhao, G.-Z., & Xu, J.-L. (2010). Electromagnetic coseismic effect associated with aftershock of Wenchuan Ms 8.0 earthquake. *Chinese Journal of Geophysics, 53,* 526–534.

Ujihara, N., Honkura, Y., & Ogawa, Y. (2004). Electric and magnetic field variations arising from the seismic dynamo effect for aftershocks of the M7.1 earthquake of 26 May 2003 off Miyagi Prefecture, NE Japan. *Earth, Planets and Space, 56*(2), 115–123.

Uyeda, S., Nagao, T., & Kamogawa, M. (2009). Short-term earthquake prediction: Current status of seismo-electromagnetics. *Tectonophysics, 470*(3), 205–213.

Uyeda, S., Nagao, T., Orihara, Y., Yamaguchi, T., & Takahashi, I. (2000). Geoelectric potential changes: Possible precursors to earthquakes in Japan. *Proceedings of the National Academy of Sciences, 97*(9), 4561–4566.

Varotsos, P., & Alexopoulos, K. (1984). Physical properties of the variations of the electric field of the earth preceding earthquakes. *I, Tectonophysics, 110*(1), 73–98.

Varotsos, P., Alexopoulos, K., & Lazaridou, M. (1993). Latest aspects of earthquake prediction in Greece based on seismic electric signals. *II, Tectonophysics, 224*(1), 1–37.

Varotsos, P., & Lazaridou, M. (1991). Latest aspects of earthquake prediction in Greece based on seismic electric signals. *Tectonophysics, 188*(3), 321–347.

Varotsos, P., Sarlis, N., Lazaridou, M., & Kapiris, P. (1998). Transmission of stress induced electric signals in dielectric media. *Journal of Applied Physics, 83*(1), 60–70.

Wu, F. T., Rau, R.-J., & Salzberg, D. (1997). Taiwan orogeny: thin-skinned or lithospheric collision? *Tectonophysics, 274*(1), 191–220.

Xu, G., Han, P., Huang, Q., Hattori, K., Febriani, F., & Yamaguchi, H. (2013). Anomalous behaviors of geomagnetic diurnal variations prior to the 2011 off the Pacific coast of Tohoku earthquake (Mw9. 0). *Journal of Asian Earth Sciences, 77,* 59–65.

Yamazaki, K. I. (2012). Estimation of temporal variations in the magnetic field arising from the motional induction that accompanies seismic waves at a large distance from the epicenter. *Geophysical Journal International, 190*(3), 1393–1403.

Yu, S.-B., & Kuo, L.-C. (2001). Present-day crustal motion along the Longitudinal Valley Fault, eastern Taiwan. *Tectonophysics, 333*(1), 199–217.

Yu, S.-B., Kuo, L.-C., Punongbayan, R. S., & Ramos, E. G. (1999). GPS observation of crustal deformation in the Taiwan-Luzon. *Geophysical Research Letters, 26*(7), 923–926.

Zhang, D., Ren, H.-X., & Huang, Q.-H. (2013). Numerical simulation study of co-seismic electromagnetic signals in porous media. *Chinese Journal of Geophysics-Chinese Edition, 56*(8), 2739–2747.

(Received August 27, 2018, revised December 5, 2018, accepted December 10, 2018, Published online January 3, 2019)